Supplemental material to this article can be found at:
http://molpharm.aspetjournals.org/content/suppl/2023/08/17/molpharm.122.000643.DC1
1521-0111/104/5/195–202$35.00
MOLECULAR PHARMACOLOGY
dx.doi.org/10.1124/molpharm.122.000643
Mol Pharmacol 104:195–202, November 2023

Development of a Selective and High Affinity Radioligand, [^{3}H]VU6013720, for the M_4 Muscarinic Receptor

Aidong Qi, Haley E. Kling, Natasha Billard, Alice L. Rodriguez, Li Peng, Jonathan W. Dickerson, Julie L. Engers, Aaron M. Bender, Mark S. Moehle, Craig W. Lindsley, Jerri M. Rook, and Colleen M. Niswender

Department of Pharmacology and Warren Center for Neuroscience Drug Discovery (A.Q., H.E.K., N.B., A.L.R., L.P., J.W.D., J.L.E., A.M.B., C.W.L., J.M.R., C.M.N.) and Department of Chemistry (C.W.L.), Vanderbilt University, Nashville, Tennessee; Vanderbilt Kennedy Center, Vanderbilt University Medical Center, Nashville, Tennessee (C.M.N); Vanderbilt Brain Institute (C.M.N.) and Vanderbilt Institute of Chemical Biology (C.W.L., C.M.N.),Vanderbilt University School of Medicine, Nashville, Tennessee; and Department of Pharmacology and Therapeutics and Center for Translational Research in Neurodegeneration (M.S.M.), University of Florida, Gainesville, Florida

Received November 2, 2022; accepted August 14, 2023

ABSTRACT

M_4 muscarinic receptors are highly expressed in the striatum and cortex, brain regions that are involved in diseases such as Parkinson's disease, schizophrenia, and dystonia. Despite potential therapeutic advantages of specifically targeting the M_4 receptor, it has been historically challenging to develop highly selective ligands, resulting in undesired off-target activity at other members of the muscarinic receptor family. Recently, we have reported first-in-class, potent, and selective M_4 receptor antagonists. As an extension of that work, we now report the development and characterization of a radiolabeled M_4 receptor antagonist, [^{3}H]VU6013720, with high affinity (pK_d of 9.5 ± 0.2 at rat M_4, 9.7 at mouse M_4, and 10 ± 0.1 at human M_4 with atropine to define nonspecific binding) and no significant binding at the other muscarinic subtypes. Binding assays using this radioligand in rodent brain tissues demonstrate loss of specific binding in *Chrm4* knockout animals. Dissociation kinetics experiments with various muscarinic ligands show differential effects on the dissociation of [^{3}H]VU6013720 from M_4 receptors, suggesting a binding site that is overlapping but may be distinct from the orthosteric site. Overall, these results demonstrate that [^{3}H]VU6013720 is the first highly selective antagonist radioligand for the M_4 receptor, representing a useful tool for studying the basic biology of M_4 as well for the support of M_4 receptor-based drug discovery.

SIGNIFICANCE STATEMENT

This manuscript describes the development and characterization of a novel muscarinic (M) acetylcholine subtype 4 receptor antagonist radioligand, [^{3}H]VU6013720. This ligand binds to or overlaps with the acetylcholine binding site, providing a highly selective radioligand for the M_4 receptor that can be used to quantify M_4 protein expression in vivo and probe the selective interactions of acetylcholine with M_4 versus the other members of the muscarinic receptor family.

Introduction

The five subtypes of muscarinic (M) acetylcholine receptors mediate a wide variety of physiologic functions and pathophysiological processes. The M_1, M_3, and M_5 subtypes are preferentially coupled to $G_{q/11}$ G proteins and activate phospholipase C, which catalyzes the phosphatidylinositol trisphosphate cascade and leads to activation of protein kinase C and intracellular Ca^{2+} mobilization. In contrast, the M_2 and M_4 subtypes are coupled to $G_{i/o}$ and inhibit adenylyl cyclase activity and reduce cyclic AMP production upon activation; additionally, signaling downstream of these receptors also modulates ion channels (Ashkenazi et al., 1988; Peralta et al., 1988; Offermanns et al., 1994; Ishii and Kurachi, 2006; Lebois et al., 2018). Muscarinic acetylcholine receptor subtypes are distributed in both the central nervous system and periphery. Although non-selective muscarinic receptor antagonists have shown therapeutic potential for the treatment of certain neurologic disorders, usage has been limited due to intolerable side effects resulting from their broad inhibition of all the muscarinic receptor subtypes (Fahn et al., 1990; Cloud and Jinnah, 2010). This has led to the development of subtype-selective ligands to improve efficacy while reducing side effects.

Of the muscarinic receptors, the M_4 subtype is most highly expressed in striatum, cortex, and some subcortical regions, such as the thalamus (Brann et al., 1988; Buckley et al., 1988; Weiner et al., 1990). It has been reported that M_4 is the primary muscarinic receptor subtype responsible for regulating

Research was supported by the National Institutes of Health [Grants R01-MH073676 and R00-NS110878], CDMRP [Grant W81XWH-19-1-0355], and Ancora Innovation, LLC.
A.M.B. and C.W.L. are inventors on applications for composition of matter patents that protect several series of M_4 antagonists.
dx.doi.org/10.1124/molpharm.122.000643.
S This article has supplemental material available at molpharm.aspetjournals.org.

ABBREVIATIONS: B_{max}, maximal binding; CHO-K1, Chinese hamster ovary K1; K_d, equilibrium dissociation constant; K_i, equilibrium inhibitory constant; M, muscarinic; NMS, N-methyl scopolamine; PAM, positive allosteric modulator; PET, positron emission tomography; WT, wild-type.

dopamine signaling and release in the basal ganglia (Gomeza et al., 1999; Jeon et al., 2010; Foster et al., 2016; Moehle et al., 2017; Moehle and Conn, 2019) and M_4 has been implicated in several neurologic disorders, such as Parkinson's disease, schizophrenia, and dystonia (Katzenschlager et al., 2003; Moehle and Conn, 2019; Moran et al., 2019).

Despite these biologic observations regarding the therapeutic potential of M_4 modulation, development of highly selective M_4 receptor orthosteric and allosteric modulators has been challenging, and, by extension, the development of radioligands specifically targeting M_4 has historically been difficult. Recently, two M_4 receptor positive allosteric modulators (PAMs), [^{11}C]-VU0467485/AZ13713945 (Deng et al., 2019) and [^{18}F]-M4R-1911 (Deng et al., 2020) have been radiolabeled and demonstrated to specifically bind to M_4 receptors. Another M_4 PAM radioligand, [^{18}F]12, has also been shown to display species' differences in terms of its binding specificity and selectivity (Haider et al., 2023). Encouragingly, the M_4 receptor PAM radioligand [^{11}C]MK-6884 has been recently reported to specifically bind to the M_4 receptor and penetrate into the brain and has been used clinically as a positron emission tomography (PET) ligand (Tong et al., 2020; Li et al., 2022). In this report, we complement these selective M_4 PAM radioligands with [^{3}H]VU6013720, a highly selective M_4 antagonist radioligand.

Recently, our group successfully synthesized and characterized several highly selective M_4 receptor antagonists, VU6013720, VU6021302, and VU6021625 (Moehle et al., 2021), VU6028418 (Spock et al., 2021), and VU6015241 (Bender et al., 2022). Of these compounds, VU6013720 exhibited the best in vitro functional potency (rat M_4 IC_{50} = 20 nM, human M_4 IC_{50} = 0.6 nM from calcium mobilization assays) as well as a good selectivity profile among the muscarinic receptor family, with IC_{50} values of >10,000 nM at rM_3 and rM_5. At rM_1, VU6013720 exhibited a functional IC_{50} of 1700 nM, displaying ~85-fold selectivity, while VU6013720 had an IC_{50} of 670 nM at rM_2, displaying ~34-fold selectivity. Additionally, the compound exhibited unbound percentages of 24% and 31% in rat and mouse plasma, as well as 5% in both rat and mouse brain tissue.

In the current report, we generated a tritiated form of this compound, [^{3}H]VU6013720. As shown here, [^{3}H]VU6013720 selectively binds to M_4 receptors with little to no binding to the M_1, M_2, M_3, and M_5 receptor subtypes. Binding assays with brain tissue homogenates reveal that [^{3}H]VU6013720 exhibits specific binding in extracts from cortex and striatum. As other existing radioligands bind to allosteric sites, it is anticipated that a selective antagonist radioligand that interacts with the acetylcholine binding site should provide a valuable tool to explore selective binding of acetylcholine to the M_4 receptor in native tissues, in vivo, in physiologic and pathophysiological disease states and for selective M_4 receptor drug development.

Materials and Methods

Cell Culture and Membrane Preparation. Chinese hamster ovary (CHO-K1) cells were purchased from the American Tissue Culture Collection (ATCC, Manassas, Virginia). CHO-K1 cells stably express rat, human, or mouse muscarinic receptors (M_1–M_5); for M_2 and M_4, cells were co-transfected with G_{qi5}. Cells were cultured in F12 medium containing 10% fetal bovine serum, 20 mM 4-(2-hydroxyethyl)-1-piperazine ethanesulfonic acid, and 1X Antibiotic/Antimycotic (contains 10,000 units/ml of penicillin, 10,000 μg/ml of streptomycin, and 25 μg/ml of Gibco Amphotericin B; Thermo Fisher Scientific, Waltham, MA) at 37°C in the presence of 5% carbon dioxide. Cells were monitored by periodical polymerase chain reaction detection using a LookOut Mycoplasma Polymerase Chain Reaction Detection Kit (Sigma-Aldrich, St Louis, MO) to eliminate potential mycoplasma infection and cells were not mycoplasma positive for the studies described here.

Cell membranes were made as previously reported (O'Brien et al., 2018; Moehle et al., 2021). CHO-K1 cells stably expressing different muscarinic receptor subtype were seeded in 150-mm dishes and allowed to grow to approximately 80–90% confluence. Cells were washed once with ice-cold phosphate-buffered saline, scraped from the dishes, and collected using a 5-minute centrifugation at 1000 g. The supernatant was removed, and the cell pellet was stored at −80°C. To prepare membrane protein, cell pellets were thawed, re-suspended in membrane binding buffer (20 mM 4-(2-hydroxyethyl)-1-piperazine ethanesulfonic acid with 10 mM $MgCl_2$ and 10 mM NaCl, pH 7.4), and homogenized using two 15-second bursts from a TR-10 polytron (Tekmar, Vernon, BC, Canada). Cell lysates were then centrifuged at 1000g for 10 minutes at 4°C, and the pellet was discarded. The resultant supernatant was centrifuged at 20,000 g for 30 minutes at 4°C and the supernatant was discarded. The remaining pellet was re-suspended in membrane binding buffer. The protein concentration was determined by bicinchoninic acid assay (Thermo Scientific, Rockford, IL). Membranes were then stored at −80°C until use.

Radiochemistry. The synthesis of VU6013720 has been reported previously (Moehle et al., 2021). Cold VU6013720 compound was radiolabeled by RC TriTec (Teufen, Switzerland) with photocatalytic H/T exchange (Fig. 1), with the [^{3}H] label most likely in the alpha position of the tertiary amine. The final radioligand, [^{3}H]VU6013720, had a purity >98% with a specific activity 23.6 Ci/mmol (233.8 GBq/mmol) and a concentration of 1 mCi/ml (37 MBq/ml). [^{3}H]NMS was manufactured on 03/08/2018, Specific activity: 80.0 Ci/mmol, Dilution: 1 mCi/ml (PerkinElmer, Boston, MA).

[^{3}H]VU6013720 Saturation Binding Assays. Saturation binding experiments were performed to determine the specificity of [^{3}H]VU6013720 binding to the muscarinic receptor subtypes. Briefly, 10 μg CHO-K1 cell membranes expressing each receptor were incubated with [^{3}H]VU6013720 in deep 96-well plates (Corning, New York) on a shaker at room temperature for 3 hours in a reaction volume of 500 μl. Saturation binding experiments were performed in triplicate or duplicate, and nonspecific binding was assessed by addition of 10 μM atropine or VU6013719 (VU6013720 structural analog, Supplemental Fig. 1). The reactions were terminated by vacuum filtration onto Unifilter-96 GF/B plate through a 96-well harvester. The filters were washed three times with cold membrane harvesting buffer (50 mM Tris-HCl and 0.9% NaCl, pH 7.4). Plates were then dried overnight and 40 μl of MicroScint 20 (PerkinElmer) was added to each well. The membrane-bound radioactivity was determined using a TopCount NXT microplate scintillation and luminescence counter (PerkinElmer). Calculation of specific binding versus total counts

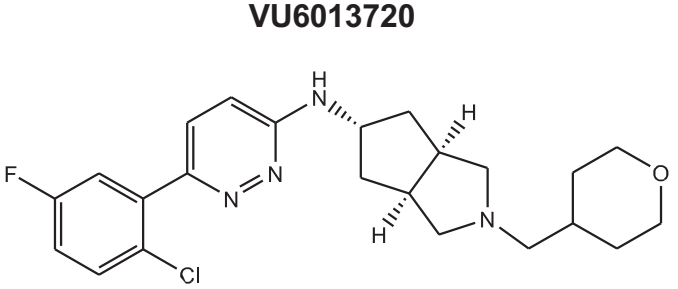

Fig. 1. Structure of VU6013720. Cold VU6013720 was labeled using nonspecific hydrogen/tritium exchange with 99% tritium gas (RC Tritec, Switzerland) with a specific activity of 23.6 Ci/mmol.

revealed that radioligand depletion was not a factor in these studies using this assay protocol.

Competition Binding Assays with [^{3}H]NMS and [^{3}H]VU6013720. Radioligand competition binding assays were performed as previously described (Moehle et al., 2021) using concentrations of radioligand that were within 2-fold of the calculated equilibrium dissociation constant (K_d). Briefly, M_4 antagonists were 1:3 serially diluted into membrane binding buffer and added to each well of a 96-well plate, along with 10 μg/well cell membrane and approximately 100 pM [^{3}H]-*N*-methylscopolamine ([^{3}H]NMS, PerkinElmer, Boston, MA) or 100 - 400 pM [^{3}H]VU6013720 in a reaction volume of 500 μl. Following a 3-hour incubation period on a shaker at room temperature, the membrane-bound ligand was separated from free ligand by filtration through glass fiber 96-well filter plates (Unifilter-96, GF/B; PerkinElmer, Boston, MA) using a 96-well Brandel harvester. The filters were washed three times with cold membrane harvesting buffer (50 mM Tris-HCl and 0.9% NaCl, pH 7.4). Plates were then dried overnight and 40 μl of MicroScint 20 (Perkin Elmer) was added to each well. The membrane-bound radioactivity was determined using a TopCount NXT microplate scintillation and luminescence counter (PerkinElmer). Nonspecific binding was determined using 10 μM atropine.

Kinetic Studies. Kinetic studies of [^{3}H]VU6013720 association/dissociation from M_4 receptors were performed at room temperature. For association assays, membranes were incubated with [^{3}H]VU6013720 at concentrations 2-fold over the K_d value for 0, 2, 5, 10, 20, 30, 45, 60, 90, 120, 150, and 180 minutes. For dissociation assays, membranes and [^{3}H]VU6013720 were allowed to equilibrate for 120 minutes and then 10 μM of cold competitor was added at 120, 90, 60, 45, 30, 20, 15, 10, 5, 2, and 1 minute before termination of the assay. Following these pretreatment times, membranes were immediately harvested by quick filtration to a GF/B plate using ice-cold harvesting buffer and a 96-well Brandel harvester. Buffer and temperature conditions for all binding studies were the same.

Animals. Male and female wildtype (two male and two female) or *Chrm4* knockout (two male and two female) mice (bred in-house) and male Sprague Dawley ($n = 4$) rats (Envigo, Indianapolis, IN) were used for this study. They were housed in the animal care facility certified by the American Association for the Accreditation of Laboratory Animal Care under a 12-hour light/dark cycle (lights on: 7 AM; lights off: 7 PM). The experimental protocols performed during the light cycle were approved by the Institutional Animals Care and Use Committee of Vanderbilt University and conformed to the guidelines established by the National Research Council Guide for the Care and Use of Laboratory Animals.

Brain Tissue Membrane Preparation and In Vitro Saturation Binding. Rats and mice (wild-type and *Chrm4* knockout) were anesthetized by continuous isoflurane (5%) and killed by decapitation, and striatum and cortex were dissected on ice. The dissected brain regions were weighed and homogenized at a concentration of 1 mg of tissue per 25 volumes of membrane binding buffer with a polytron for two 20-second bursts. The homogenates were centrifuged at 20,000 g for 20 minutes at 4°C, and the supernatant was discarded. The pellet was homogenized in membrane binding buffer and centrifuged under the same conditions as above. The final homogenate was re-suspended in membrane binding buffer and incubated at 37°C for 10 minutes and centrifuged as above. The resultant pellet was re-suspended in membrane binding buffer, and the protein concentration was determined by bicinchoninic acid assay. The brain homogenate was stored at −80°C until use. To determine the specific binding of [^{3}H]VU6013720 using brain tissue membranes, saturation assays were performed as above with CHO cell membranes but using 150 μg of brain homogenate protein per well.

Data Analysis. All experiments were carried out in duplicate or triplicate and were performed at least three times (unless stated otherwise), which aligns with our historical and standard assay protocol. Studies presented in this manuscript are exploratory in nature and were performed to characterize a new radioligand of general interest to scientists interested in the biology of the muscarinic receptors. Data were analyzed using GraphPad Prism (GraphPad Software, San Diego, CA) with the following equations and were not constrained at the top or bottom.

Saturation Binding. Nonspecific binding at each radioligand concentration was subtracted from total binding and the data were fit to the following equation:

$$\text{Specific Binding} = (B_{max} * [L]) / (K_d + [L]), \text{where}$$

$$[L] \text{ is the concentration of free radioligand in nM} \quad (1)$$

Competition Binding. Data were analyzed using the Cheng Prusoff equation:

$$K_i = IC_{50} / (1 + [\text{radioligand}] / K_d) \quad (2)$$

Association Kinetics. Y=Y0 + (Plateau-Y0)*(1-exp(-K*x)), where Y0 is the Y value when time (X) is 0, expressed as % [^{3}H]VU6013720 binding; plateau is the Y value at infinite time, expressed as % [^{3}H]VU6013720 binding; K is the rate constant, expressed as inverse minutes; Tau is the time constant, expressed in minutes; half-time is calculated as ln(2)/K, expressed as minutes, and span is the difference between Y0 and Plateau, expressed as % [^{3}H]VU6013720 binding.

Dissociation Kinetics: One-Phase or Two-Phase Exponential Decay. One phase: Y=(Y0-NS)*exp(-K*X) + NS, where Y0 is the binding at time zero, expressed as % [^{3}H]VU6013720 binding; NS is nonspecific binding at infinite time, expressed as % [^{3}H]VU6013720 binding; K is the rate constant in inverse minutes; half-time equals ln(2) divided by K.

$$\text{Two phase: } Span_{Fast} = (Y0 - Plateau) * Percent_{Fast} * .01$$

$$Span_{Slow} = (Y0 - Plateau) * (100 - Percent_{Fast}) * .01$$

$$Y = Plateau + Span_{Fast} * \exp(-K_{Fast} * X) + Span_{Slow} * \exp(-K_{Slow} * X) \quad (3)$$

where Y0 is the Y value when X (time) is zero, expressed as % [^{3}H]VU6013720 binding; plateau is the Y value at infinite time, expressed in minutes; Kfast and Kslow are the rate constants, expressed as inverse minutes; time units; TauFast and TauSlow are the two time constants, expressed as time; Half-life (fast) and Half-life (slow) are computed as ln(2)/K and expressed as minutes; PercentFast is the fraction of the span (from Y0 to Plateau) accounted for by the faster of the two components.

Data from individual experiments were fit independently and then presented as the pIC_{50} or pK_i/pK_d as mean ± standard deviation. Data shown in the figures represents either combined data from multiple experiments or, in some cases, as a data set from a typical experiment as noted in the various figure legends.

Results

VU6013720 is a Selective M_4 Antagonist. VU6013720 (Fig. 1) binding affinities and subtype selectivity at the five rat muscarinic receptor subtypes were assessed using binding competition against the non-selective orthosteric radioligand [^{3}H]N-methylscopolamine (NMS) in membranes made from CHO-K1 cells expressing each receptor subtype (Table 1; Fig. 2). VU6013720 fully displaced [^{3}H]NMS binding from rat M_4 receptors with a pK_i of 8.8 ± 0.1 ($n = 4$), while equilibrium inhibitory constant (pK_i) values were 6.9 ± 0.2 ($n = 4$) for M_2 and affinity values were above a micromolar for M_1, M_3, and M_5. The ratio of the nanomolar K_i value at the receptor with the closest binding affinity, M_2, versus M_4 was 80-fold. These competition binding data, together with IC_{50} values from calcium mobilization assays (Moehle et al., 2021), demonstrate that VU6013720 is a highly selective M_4 antagonist with

TABLE 1
Characterization of the binding specificity of VU6013720 using the orthosteric muscarinic antagonist radioligand [^{3}H]-N-methylscopolamine pK_i values were obtained from [^{3}H]-NMS competition binding assays with CHO-K1 cell membranes expressing different rat muscarinic receptor subtypes. Data represent the mean ± S.D. of four independent experiments performed in triplicate and refer to the curve fits in Fig. 2.

	pK_i (mean ± S.D.)	K_i (nM)	Selectivity (fold over M_4 K_i)
M_4	8.8 ± 0.0	1.6	
M_1	5.7 ± 0.1	2000	1300
M_2	6.9 ± 0.2	130	80
M_3	5.6 ± 0.2	2500	1600
M_5	5.5 ± 0.1	3100	2000

single-digit nanomolar affinity, and possesses the characteristics needed to move to further characterization as a radioligand.

[^{3}H]VU6013720 Binds Specifically to M_4 Receptors with High Affinity. We radiolabeled VU6013720 and determined the interaction of this novel radioligand across the muscarinic receptor family using saturation binding assays performed with cell membranes expressing the various receptor subtypes. Nonspecific binding was determined in the presence of a structurally related antagonist, VU6013719 (Supplemental Fig. 1; synthesis provided in Supplemental Methods), or the nonselective muscarinic antagonist, atropine. [^{3}H]VU6013720 bound specifically to the rat M_4 receptor with a pK_d of 9.7 ± 0.2 (Fig. 3A; Table 2) and a B_{max} of 4800 ± 500 fmol/mg using VU6013719 as the nonspecific binding control ($n = 4$) and a pK_d of 9.5 ± 0.2 and a B_{max} of 4100 ± 500 fmol/mg using atropine (Fig. 3B; Table 2, $n = 3$). These values were slightly different when compared with the pK_i determined with [^{3}H]NMS (8.8 versus 9.7/9.5), which may suggest differential interaction of [^{3}H]VU6013720 and [^{3}H]NMS with the receptor. In contrast, [^{3}H]VU6013720 exhibited no specific binding at the rat M_1, M_2, M_3, and M_5 receptor subtypes (Fig. 3, C–F, $n = 3$ per receptor). These data suggest that [^{3}H]VU6013720 binds specifically to the M_4 receptor with high affinity. We performed a comparison of the pK_i value of atropine with both [^{3}H]NMS and [^{3}H]VU6013720 and found the pK_i to be statistically different between the two radioligands (8.7 ± 0.1 with [^{3}H]NMS and 9.0 ± 0.1 with [^{3}H]VU6013720, mean ± S.D., $^{**}P = 0.009$). As these two radioligands are of different structure, this would suggest that the binding sites of the two, or the binding pose adopted by atropine in the presence of each radioligand, are not exactly the same. We also compared B_{max} values for saturation binding studies of [^{3}H]NMS and [^{3}H]VU6013720 and determined B_{max} values of 4500 ± 700 and 4100 ± 500 fmol/mg (Supplemental Fig. 2, paired Student's t test, $P = 0.219$, $n = 3$), respectively, suggesting that the two radioligands label a similar number of binding sites on the receptor. To assess cross-species binding of [^{3}H]VU6013720, saturation binding was also assayed with membranes expressing the human and mouse M_4 receptors. Similar to the rat M_4 receptor, [^{3}H]VU6013720 bound to these receptors with high affinity, with

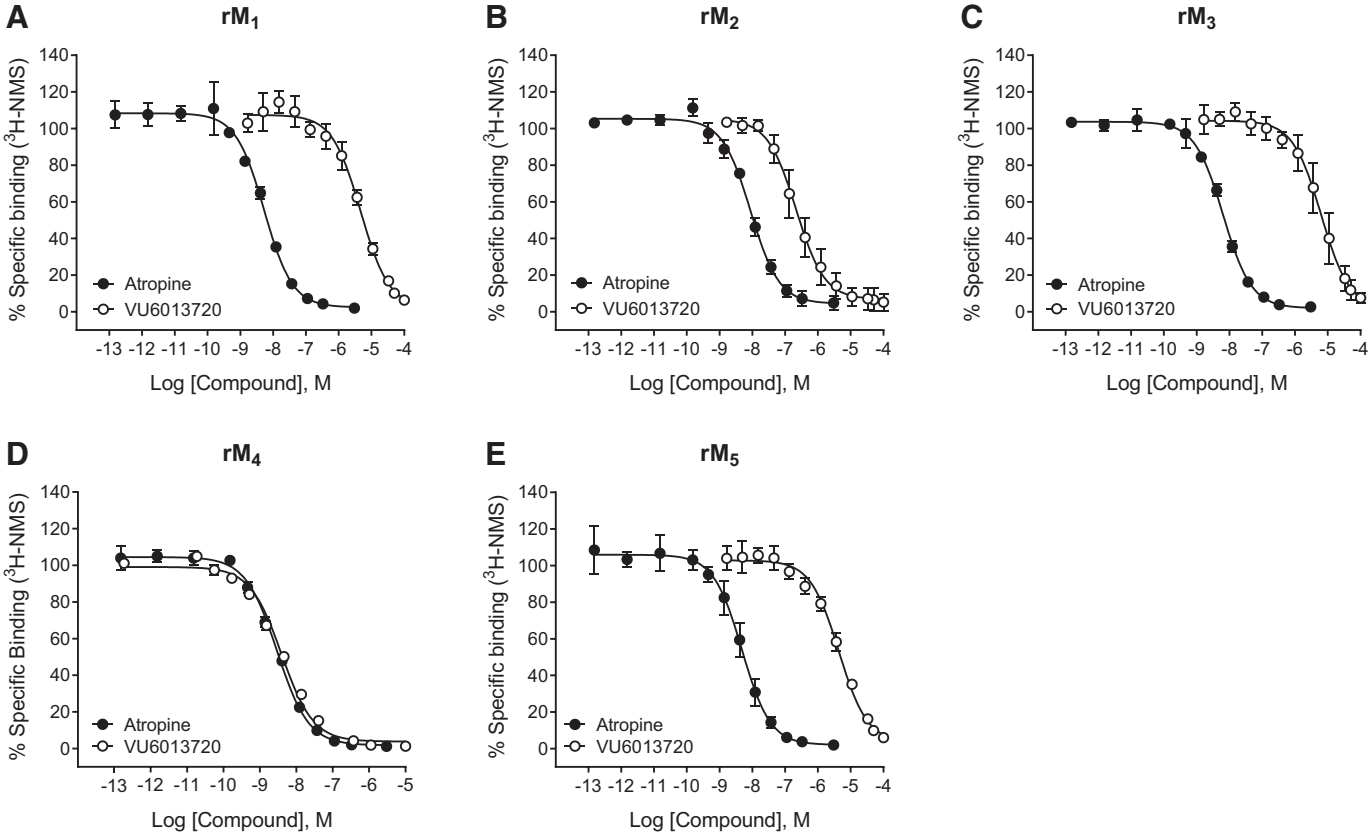

Fig. 2. Binding selectivity of VU6013720 at muscarinic acetylcholine receptor subtypes using [^{3}H]NMS. VU6013720 and atropine competition binding curves at various muscarinic acetylcholine receptor subtypes were performed using the orthosteric muscarinic radioligand, [^{3}H]-N-methylscopolamine. Data are the mean ± S.D. from a representative of four independent experiments performed in triplicate.

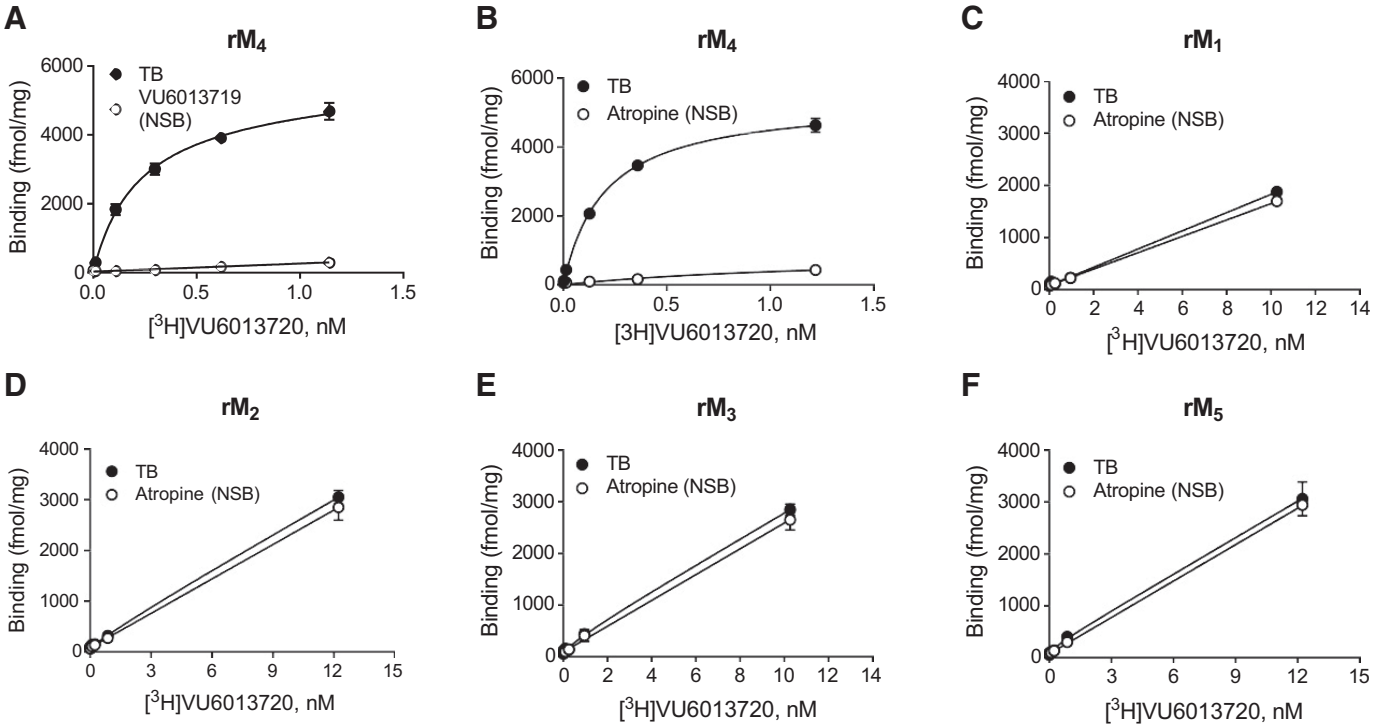

Fig. 3. Among the five muscarinic receptors, [^{3}H]VU6013720 binds specifically to the rat M_4 receptor. Total and specific binding for [^{3}H]VU6013720 was determined using cells expressing each of the rat muscarinic receptors. [^{3}H]VU6013720 bound specifically to the rat M_4 receptor in a saturable manner using either VU6013719 (A) or atropine (B) as nonspecific binding controls, whereas no detectable binding was observed at rat M_1, M_2, M_3, or M_5 using atropine to determine nonspecific binding (C–F). Data shown are the mean ± S.D. of a representative of at least three independent experiments performed in triplicate.

pK_d values of 10 ± 0.1 (n = 3) at the human M_4 receptor and 9.7 at the mouse M_4 receptor, respectively (n = 1, Supplemental Fig. 3; Table 2).

Kinetic Evaluation of [^{3}H]VU6013720. To fully characterize this novel radioligand, kinetic binding studies examining association and dissociation were next conducted using a concentration of radioligand calculated to be within 2-fold of the K_d in each experiment. Association experiments demonstrated that [^{3}H]VU6013720 binding reached equilibrium within 10 minutes (Fig. 4A) with an association on-rate of 1.7 ± 0.1 $nM^{-1}min^{-1}$ (n = 3). [^{3}H]VU6013720 dissociated completely by adding 10 μM VU6013719 or atropine, although with distinct time courses (Fig. 4B; Table 3, n = 3). The data for both of these compounds was better fit to a two-site decay model versus a single site. We observed faster dissociation with the structural analog VU6013719 than atropine (Table 3), suggesting that [^{3}H]VU6013720 and VU6013719 may share a binding site that is distinct or overlapping that of atropine. We also examined dissociation kinetics induced by the positive allosteric modulator, VU0467154 (Bubser et al., 2014). VU0467154 induced partial but saturable displacement of [^{3}H]VU6013720, similar to what we had previously observed with [^{3}H]NMS (Bubser et al., 2014). This suggests that VU0467154 is binding to an allosteric site but induces negative cooperativity with [^{3}H]VU6013720 by partially displacing the ligand.

[^{3}H]VU6013720 Specifically Binds to M_4 in the Rodent Brain. One of the main advantages of a highly specific radioligand is sensitivity for detection of receptors in native tissues. To determine the utility of [^{3}H]VU6013720 for detecting M_4 receptors in brain tissue, membranes were prepared from the striatum and cortex of rats. As shown in Fig. 5, saturation binding assays detected specific binding of [^{3}H]VU6013720 to homogenates from rat striatum and cortex with high affinities (pK_d = 9.0 ± 0.2 in cortex, (n = 3, A)) and 9.3 ± 0.2 in striatum, (n = 3, B)). B_{max} values of 260 ± 110 (cortex) and 350 ± 60 (striatum) fmol/mg protein were also determined (n = 3). We would note that, when the pK_d values for rat M_4 cells, cortex, and striatum were compared using a one- way ANOVA, there was a significant difference ($P < 0.05$) between rat M_4 cells and the cortex, but not the striatum. This may reflect distinct microenvironments between an in vitro cell system versus the brain.

To further confirm that these binding sites were indeed M_4 receptors, saturation binding was also performed with membranes made from both wild-type (WT) and *Chrm4*

TABLE 2
Summary of binding properties of [^{3}H]VU6013720 at multiple species of M_4 receptor
Data represent mean ± S.D. from at least four experiments performed in quadruplicate (human and rat) and one experiment (mouse) performed in triplicate. # and @ denote the use of VU6013719 and atropine, respectively, for non-specific binding. Data refer to saturation binding curves shown in Fig. 3 and Supplemental Fig. 3.

[^{3}H]-VU6013720	Human M_4[#]	Mouse M_4[#]	Rat M_4[#]	Rat M_4[@]
pK_d	10 ± 0.1	9.7	9.7 ± 0.2	9.5 ± 0.2
B_{max} (fmol/mg)	1200 ± 40	1400	4800 ± 500	4100 ± 500

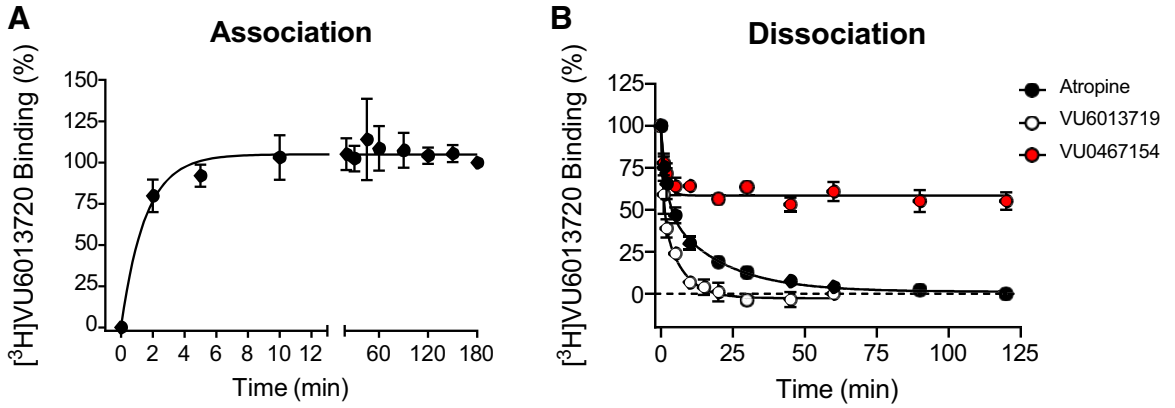

Fig. 4. Kinetic characterization of the [^{3}H]VU6013720 radioligand. Time course experiments defining association and dissociation of [^{3}H]VU6013720 at rat M_4 membranes were performed at room temperature. (A) Association was initiated by addition of [^{3}H]VU6013720 to membranes at the indicated time points before filtration. (B) Dissociation experiments were performed by allowing [^{3}H]VU6013720 to equilibrate with membranes for 2 hours; at this point, a 10 μM final concentration of VU6013719 (white), atropine (black), or VU0467154 (red) was added at designated times before terminating the reaction by filtration. Data are the mean ± S.D. of three independent experiments performed in triplicate.

knockout mouse cortex. As shown in Fig. 5, C and D, [^{3}H]VU6013720 specifically bound to WT mouse cortex and exhibited essentially no binding to cortical membranes from *Chrm4* knockout mice. These data demonstrate that [^{3}H]VU6013720 is a useful tool for quantification of M_4 receptors in brain tissue.

Discussion

M_4 muscarinic receptors are highly expressed in the brain (e.g., striatum, cortex, thalamus) and have been demonstrated to be involved in several central nervous system diseases (Pancani et al., 2015; Felder et al., 2018; Moehle and Conn, 2019; Teal et al., 2019; Dean and Scarr, 2020; Foster et al., 2021; Moehle et al., 2021). Lack of selective muscarinic receptor antagonists has prevented the utilization of antimuscarinic therapy due to intolerable adverse effects, and tools that assist with drug discovery efforts, such as highly specific radioligands, may open new avenues for exploration. Here, we demonstrate that [^{3}H]VU6013720 is a novel, high-affinity, highly specific antagonist radioligand for the M_4 receptor. [^{3}H]VU6013720 selectively binds to the M_4 receptor with pK_d values of 9.5 at rat, 10 at human, and 9.7 at mouse M_4 receptors. Based on this profile, we used this high-affinity radioligand to quantify M_4 receptors in brain tissue by saturation binding with brain tissue homogenates.

There are some interesting, subtle findings from the current studies. While the majority of our data point to an orthosteric or overlapping binding site for VU6013720, the pK_i for cold VU6013720 is 8.8 at rat M_4 using [^{3}H]NMS binding while the pK_d was calculated to be 9.5 with atropine and 9.7 with VU6013719. Additionally, competition binding studies using VU6013720 itself revealed a pK_i of 9.5 (data not shown), which is close to the K_d value. When considered in the context of the significant shift of the pK_i of atropine between [^{3}H]NMS and [^{3}H]VU6013720, it suggests that these two radioligands might make distinct contacts within similar, but not identical, binding sites. This is further supported by the dissociation kinetics experiments in which the dissociation of [^{3}H]VU6013720 differs in the presence of atropine versus VU6013719. Other factors may impact these results, such as differences in residence time. The discrepancy between pK_is for atropine with the two radioligands at M_4 also suggested the possibility that, due to the high sequence conservation, a similar leftward affinity shift might exist for M_2 which might have resulted in specific binding at M_2; however, we did not observe any saturable binding to this receptor subtype.

We previously reported a 30-fold selectivity difference for the human and rat M_4 receptors for VU6013720 in a chimeric G protein assay that allows the M_4 receptor to couple to calcium mobilization (Moehle et al., 2021). In contrast, our data here show that there is only a 3-fold difference in affinity between the human and rat M_4 receptors. We currently do not have an explanation for this difference, although there are several possibilities. First, the functional assays include acetylcholine, whereas the binding assays do not. If VU6013720 is truly orthosteric, this should not be a confound; however, if ACh/NMS and VU6013720 have subtly different binding

TABLE 3

Dissociation kinetics of [^{3}H]VU6013720 induced by multiple ligands

Dissociation was performed by adding 10 μM of atropine, VU6013719, or VU0467154 at designated times. Data were fit with both one- and two-phase decay curves. For atropine and VU6013719, two-site fits were the preferred model; for VU0467154, a one-site model was preferred. *$P < 0.05$, **$P < 0.01$, ***$P < 0.001$ between atropine and VU6013719.

	% Fast	K_{off} fast (min^{-1})	K_{off} slow (min^{-1})	Half-life fast (min)	Half-life slow (min)	Plateau	R^2
Atropine	51 ± 5	0.56 ± 0.39	0.05 ± 0.01	1.6 ± 0.9	15 ± 3	1.0 ± 0.7	0.98 ± 0.02
VU6013719	44 ± 8	2.0 ± 0.5*	0.17 ± 0.02***	0.40 ± 0.10	4.2 ± 0.5**	−2.2 ± 3.2	0.98 ± 0.01
		K_{off} (min^{-1})		Half-life (min)		Plateau	R^2
VU0467154		0.60 ± 0.18		1.2 ± 0.3		58 ± 5	0.84 ± 0.05

K_{off}, dissociation off rate.

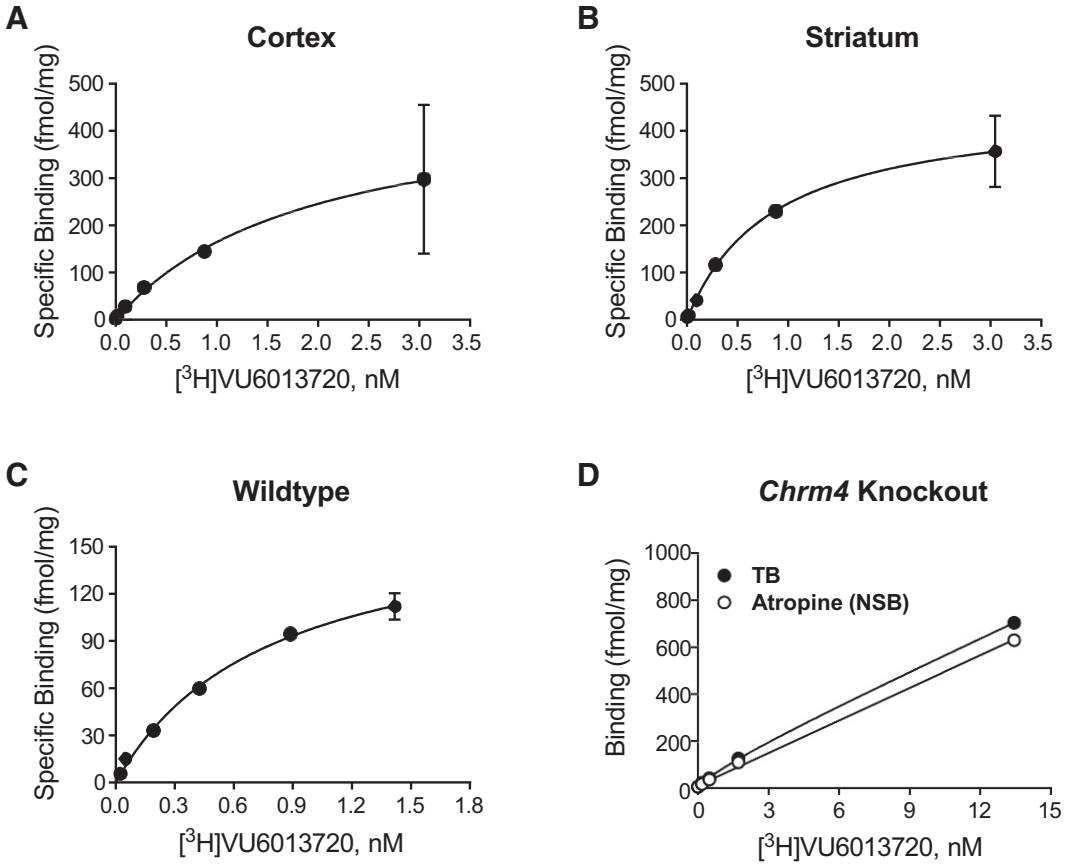

Fig. 5. [^{3}H]VU6013720 binds specifically to rat brain cortical and striatal tissue as well as to cortical membranes from WT but not from *Chrm4* knockout mice. Rat cortical (A) and striatal (B) homogenates were incubated with [^{3}H]VU6013720 in the presence and absence of 10 μM atropine to determine total and nonspecific binding. [^{3}H]VU6013720 bound to rat cortical membranes with a pK_d of 9.0 ± 0.2 and a B_{max} of 260 ± 110 fmol/mg of protein and to rat striatal membranes with a pK_d of 9.3 ± 0.2 and a B_{max} of 350 ± 60 fmol/mg of protein. Data are mean ± S.D. and representative of three independent experiments performed in triplicate. Cortical homogenates from WT (C) and *Chrm4* knockout mice (D) were incubated with [^{3}H]VU6013720 in the presence and absence of 10 μM atropine to determine total and nonspecific binding. [^{3}H]VU6013720 binds to cortical membranes from WT mice with a pK_d of 9.0 ± 0.4 and a B_{max} of 240 ± 90 fmol/mg of protein, whereas little specific [^{3}H]VU6013720 binding was detected in cortical homogenates from *Chrm4* knockout mice. Data are the mean ± S.D. and a representative of three independent experiments performed in duplicate or triplicate.

sites and these binding sites are slightly different between the two species, this could contribute to these discrepancies. Additionally, if VU6013720 is actually an inverse agonist, its functional potency may be dissociated from its binding affinity due to G protein interactions or other protein/protein interactions that are induced in the cells when the receptor is functionally assessed. We also do not currently know if there is a species difference in terms of contact with the chimeric G protein used in these studies, G_{qi5}, and whether G_{qi5} impacts receptor conformation in binding studies. Future experiments around this issue could include assessment of VU6013720 effects in an assay in which constitutive activity of the receptor might be observed, such as inositol phosphate accumulation or cAMP generation, to determine if there is a distinction in inverse agonist activity, and further exploration of the effects of various G proteins or signaling partners.

To our knowledge, this is the first development of a broadly useful, highly specific antagonist radioligand with high affinity for M_4 receptors, and the development of [^{3}H]VU6013720 is anticipated to be a powerful tool for M_4 receptor studies. Previous approaches to investigate the tissue distribution of the M_4 receptor include RNA detection techniques, or by antibody, with confirmation using knockout tissue (Brann et al., 1988; Buckley et al., 1988; Weiner et al., 1990; Levey et al., 1991; Levey 1993; Vilaró et al., 1993; Wolfe and Yasuda, 1995; Tice et al., 1996; Gomeza et al., 1999). Although these studies provide important insight into relative distribution, detected RNA levels are not always consistent with protein expression levels, and antibodies do not provide the same level of quantitation that is possible using specific radioligand binding. As we have shown in this report, our studies using [^{3}H]VU6013720 were able to confirm and quantify the M_4 receptor protein expression pattern and receptor density levels in native brain tissues. For this reason, we anticipate that [^{3}H]VU6013720 will be an important tool for investigating the M_4 receptor distribution in native tissues and may also be useful for interrogating potential differences that may occur in different disease states or models.

In the past several years, several M_4 receptor radioligands have been reported, the M_2/M_4 PAM [^{3}H]LY2119620 (Schober et al., 2014), and the selective M_4 PAMs [^{11}C]-VU0467485/AZ13713945 (Deng et al., 2019), [^{18}F]-M4R-1911 (Deng et al., 2020), [^{11}C]MK-6884 (Tong et al., 2020), and [^{18}F]12 (Haider et al., 2023). However, these radioligands have been developed from M_4 PAM scaffolds and bind to allosteric sites on the M_4 receptor. [^{3}H]VU6013720 is the first reported selective

radiolabeled M_4 receptor antagonist. Therefore, it is a unique tool that could be paired with PAM radioligands to study compound binding sites as well as for the development of future M_4 antagonists and modulators. Additionally, the compound could potentially be used to map acetylcholine levels in the brain relevant for M_4 function and be useful for in vitro screening of M_4 antagonists for therapeutic treatment of movement disorders and may serve as a starting point for development of antagonists with higher affinity and favorable drug metabolism and pharmacokinetic properties to eventually lead to PET ligands.

In conclusion, we have developed the first highly selective M_4 receptor antagonist radioligand with high affinity for the rodent and human M_4 receptors, [^{3}H]VU6013720. A reliable tool will lead to a better understanding of the physiology and pathophysiology associated with this important signaling protein and facilitate the support of drug development for neurologic diseases for which M_4 modulators are predicted to exhibit efficacy, such as Parkinson's disease, essential tremor, and schizophrenia.

Acknowledgments

The authors thank Jeff Conn and members of the Warren Center for Neuroscience Drug Discovery for stimulating and formative discussions. The authors also thank the William K. Warren Foundation for endowing the WCNDD.

Data Availability

The authors declare that all processed data supporting the findings of this study are available within the paper and its Supplemental Materials. Raw data are available on request from the corresponding author.

Authorship Contributions

Participated in research design: Qi, Rodriguez, Dickerson, Bender, Moehle, Lindsley, Rook, Niswender.

Conducted experiments: Qi, Kling, Billard, Peng, Dickerson, Bender.

Contributed new reagents or analytic tools: Engers, Bender, Lindsley.

Performed data analysis: Qi, Rodriguez, Dickerson, Rook, Niswender.

Wrote or contributed to the writing of the manuscript: Qi, Rodriguez, Dickerson, Engers, Bender, Lindsley, Rook, Niswender.

References

Ashkenazi A, Peralta EG, Winslow JW, Ramachandran J, and Capon DJ (1988) Functional role of muscarinic acetylcholine receptor subtype diversity. *Cold Spring Harb Symp Quant Biol* **53**:263–272.

Bender AM, Carter TR, Spock M, Rodriguez AL, Dickerson JW, Rook JM, Chang S, Qi A, Presley CC, Engers DW et al. (2022) Synthesis and characterization of chiral 6-azaspiro[2.5]octanes as potent and selective antagonists of the M_4 muscarinic acetylcholine receptor. *Bioorg Med Chem Lett* **56**:128479.

Brann MR, Buckley NJ, and Bonner TI (1988) The striatum and cerebral cortex express different muscarinic receptor mRNAs. *FEBS Lett* **230**:90–94.

Bubser M, Bridges TM, Dencker D, Gould RW, Grannan M, Noetzel MJ, Lamsal A, Niswender CM, Daniels JS, Poslusney MS et al. (2014) Selective activation of M4 muscarinic acetylcholine receptors reverses MK-801-induced behavioral impairments and enhances associative learning in rodents. *ACS Chem Neurosci* **5**:920–942.

Buckley NJ, Bonner TI, and Brann MR (1988) Localization of a family of muscarinic receptor mRNAs in rat brain. *J Neurosci* **8**:4646–4652.

Cloud LJ and Jinnah HA (2010) Treatment strategies for dystonia. *Expert Opin Pharmacother* **11**:5–15.

Dean B and Scarr E (2020) Muscarinic M1 and M4 receptors: Hypothesis driven drug development for schizophrenia. *Psychiatry Res* **288**:112989.

Deng X, Hatori A, Chen Z, Kumata K, Shao T, Zhang X, Yamasaki T, Hu K, Yu Q, Ma L et al. (2019) Synthesis and Preliminary Evaluation of ^{11}C-Labeled VU0467485/AZ13713945 and Its Analogues for Imaging Muscarinic Acetylcholine Receptor Subtype 4. *ChemMedChem* **14**:303–309.

Deng X, Zhang Y, Chen Z, Kumata K, Van R, Rong J, Shao T, Hatori A, Mori W, Yu Q et al. (2020) Synthesis and preliminary evaluation of 4-hydroxy-6-(3-[(11)C]methoxyphenethyl)pyridazin-3(2H)-one, a (11)C-labeled d-amino acid oxidase (DAAO) inhibitor for PET imaging. *Bioorg Med Chem Lett* **30**:127326.

Fahn S, Burke R, and Stern Y (1990) Antimuscarinic drugs in the treatment of movement disorders. *Prog Brain Res* **84**:389–397.

Felder CC, Goldsmith PJ, Jackson K, Sanger HE, Evans DA, Mogg AJ, and Broad LM (2018) Current status of muscarinic M1 and M4 receptors as drug targets for neurodegenerative diseases. *Neuropharmacology* **136**:449–458.

Foster DJ, Bryant ZK, and Conn PJ (2021) Targeting muscarinic receptors to treat schizophrenia. *Behav Brain Res* **405**:113201.

Foster DJ, Wilson JM, Remke DH, Mahmood MS, Uddin MJ, Wess J, Patel S, Marnett LJ, Niswender CM, Jones CK et al. (2016) Antipsychotic-like Effects of M4 Positive Allosteric Modulators Are Mediated by CB2 Receptor-Dependent Inhibition of Dopamine Release. *Neuron* **91**:1244–1252.

Gomeza J, Zhang L, Kostenis E, Felder C, Bymaster F, Brodkin J, Shannon H, Xia B, Deng C, and Wess J (1999) Enhancement of D1 dopamine receptor-mediated locomotor stimulation in M(4) muscarinic acetylcholine receptor knockout mice. *Proc Natl Acad Sci USA* **96**:10483–10488.

Haider A, Deng X, Mastromihalis O, Pfister SK, Jeppesen TE, Xiao Z, Pham V, Sun S, Rong J, Zhao C et al. (2023) Structure-activity relationship of pyrazol-4-yl-pyridine derivatives and identification of a radiofluorinated probe for imaging the muscarinic acetylcholine receptor M_4. *Acta Pharm Sin B* **13**:213–226.

Ishii M and Kurachi Y (2006) Muscarinic acetylcholine receptors. *Curr Pharm Des* **12**:3573–3581.

Jeon J, Dencker D, Wörtwein G, Woldbye DPD, Cui Y, Davis AA, Levey AI, Schütz G, Sager TN, Mørk A et al. (2010) A subpopulation of neuronal M4 muscarinic acetylcholine receptors plays a critical role in modulating dopamine-dependent behaviors. *J Neurosci* **30**:2396–2405.

Katzenschlager R, Sampaio C, Costa J, and Lees A (2003) Anticholinergics for symptomatic management of Parkinson's disease. *Cochrane Database Syst Rev* **2002**:CD003735.

Lebois EP, Thorn C, Edgerton JR, Popiolek M, and Xi S (2018) Muscarinic receptor subtype distribution in the central nervous system and relevance to aging and Alzheimer's disease. *Neuropharmacology* **136**:362–373.

Levey AI (1993) Immunological localization of m1-m5 muscarinic acetylcholine receptors in peripheral tissues and brain. *Life Sci* **52**:441–448.

Levey AI, Kitt CA, Simonds WF, Price DL, and Brann MR (1991) Identification and localization of muscarinic acetylcholine receptor proteins in brain with subtype-specific antibodies. *J Neurosci* **11**:3218–3226.

Li W, Wang Y, Lohith TG, Zeng Z, Tong L, Mazzola R, Riffel K, Miller P, Purcell M, Holahan M et al. (2022) The PET tracer [^{11}C]MK-6884 quantifies M4 muscarinic receptor in rhesus monkeys and patients with Alzheimer's disease. *Sci Transl Med* **14**:eabg3684.

Moehle MS, Bender AM, Dickerson JW, Foster DJ, Qi A, Cho HP, Donsante Y, Peng W, Bryant Z, Stillwell KJ et al. (2021) Discovery of the First Selective M_4 Muscarinic Acetylcholine Receptor Antagonists with *in Vivo* Antiparkinsonian and Antidystonic Efficacy. *ACS Pharmacol Transl Sci* **4**:1306–1321.

Moehle MS and Conn PJ (2019) Roles of the M_4 acetylcholine receptor in the basal ganglia and the treatment of movement disorders. *Mov Disord* **34**:1089–1099.

Moehle MS, Pancani T, Byun N, Yohn SE, Wilson 3rd GH, Dickerson JW, Remke DH, Xiang Z, Niswender CM, Wess J et al. (2017) Cholinergic Projections to the Substantia Nigra Pars Reticulata Inhibit Dopamine Modulation of Basal Ganglia through the M_4 Muscarinic Receptor. *Neuron* **96**:1358–1372.e4.

Moran SP, Maksymetz J, and Conn PJ (2019) Targeting Muscarinic Acetylcholine Receptors for the Treatment of Psychiatric and Neurological Disorders. *Trends Pharmacol Sci* **40**:1006–1020.

O'Brien DE, Shaw DM, Cho HP, Cross AJ, Wesolowski SS, Felts AS, Bergare J, Elmore CS, Lindsley CW, Niswender CM et al. (2018) Differential Pharmacology and Binding of $mGlu_2$ Receptor Allosteric Modulators. *Mol Pharmacol* **93**:526–540.

Offermanns S, Wieland T, Homann D, Sandmann J, Bombien E, Spicher K, Schultz G, and Jakobs KH (1994) Transfected muscarinic acetylcholine receptors selectively couple to Gi-type G proteins and Gq/11. *Mol Pharmacol* **45**:890–898.

Pancani T, Foster DJ, Moehle MS, Bichell TJ, Bradley E, Bridges TM, Klar R, Poslusney M, Rook JM, Daniels JS et al. (2015) Allosteric activation of M4 muscarinic receptors improve behavioral and physiological alterations in early symptomatic YAC128 mice. *Proc Natl Acad Sci USA* **112**:14078–14083.

Peralta EG, Winslow JW, Ashkenazi A, Smith DH, Ramachandran J, and Capon DJ (1988) Structural basis of muscarinic acetylcholine receptor subtype diversity. *Trends Pharmacol Sci* (Suppl):6–11.

Schober DA, Croy CH, Xiao H, Christopoulos A, and Felder CC (2014) Development of a radioligand, [(3)H]LY2119620, to probe the human M(2) and M(4) muscarinic receptor allosteric binding sites. *Mol Pharmacol* **86**:116–123.

Spock M, Carter TR, Bollinger KA, Han C, Baker LA, Rodriguez AL, Peng L, Dickerson JW, Qi A, Rook JM et al. (2021) Discovery of VU6028418: A Highly Selective and Orally Bioavailable M_4 Muscarinic Acetylcholine Receptor Antagonist. *ACS Med Chem Lett* **12**:1342–1349.

Teal LB, Gould RW, Felts AS, and Jones CK (2019) Selective allosteric modulation of muscarinic acetylcholine receptors for the treatment of schizophrenia and substance use disorders. *Adv Pharmacol* **86**:153–196.

Tice MA, Hashemi T, Taylor LA, and McQuade RD (1996) Distribution of muscarinic receptor subtypes in rat brain from postnatal to old age. *Brain Res Dev Brain Res* **92**:70–76.

Tong L, Li W, Lo MM, Gao X, Wai JM, Rudd M, Tellers D, Joshi A, Zeng Z, Miller P et al. (2020) Discovery of [^{11}C]MK-6884: A Positron Emission Tomography (PET) Imaging Agent for the Study of M4Muscarinic Receptor Positive Allosteric Modulators (PAMs) in Neurodegenerative Diseases. *J Med Chem* **63**:2411–2425.

Vilaró MT, Mengod G, and Palacios JM (1993) Advances and limitations of the molecular neuroanatomy of cholinergic receptors: the example of multiple muscarinic receptors. *Prog Brain Res* **98**:95–101.

Weiner DM, Levey AI, and Brann MR (1990) Expression of muscarinic acetylcholine and dopamine receptor mRNAs in rat basal ganglia. *Proc Natl Acad Sci USA* **87**:7050–7054.

Wolfe BB and Yasuda RP (1995) Development of selective antisera for muscarinic cholinergic receptor subtypes. *Ann N Y Acad Sci* **757**:186–193.

Address correspondence to: Colleen M. Niswender, 1215D Light Hall, Department of Pharmacology and Warren Center for Neuroscience Drug Discovery, Vanderbilt University, Nashville, TN 37232. E-mail: colleen.niswender@vanderbilt.edu

Supplemental Data

Development of a selective and high affinity radioligand, [^{3}H]VU6013720, for the M_4 muscarinic receptor

Aidong Qi, Haley E. Kling, Natasha Billard, Alice L. Rodriguez, Li Peng, Jonathan W. Dickerson, Julie L. Engers, Aaron M. Bender, Mark S. Moehle, Craig W. Lindsley, Jerri M. Rook, and Colleen M. Niswender

Supplemental Figures

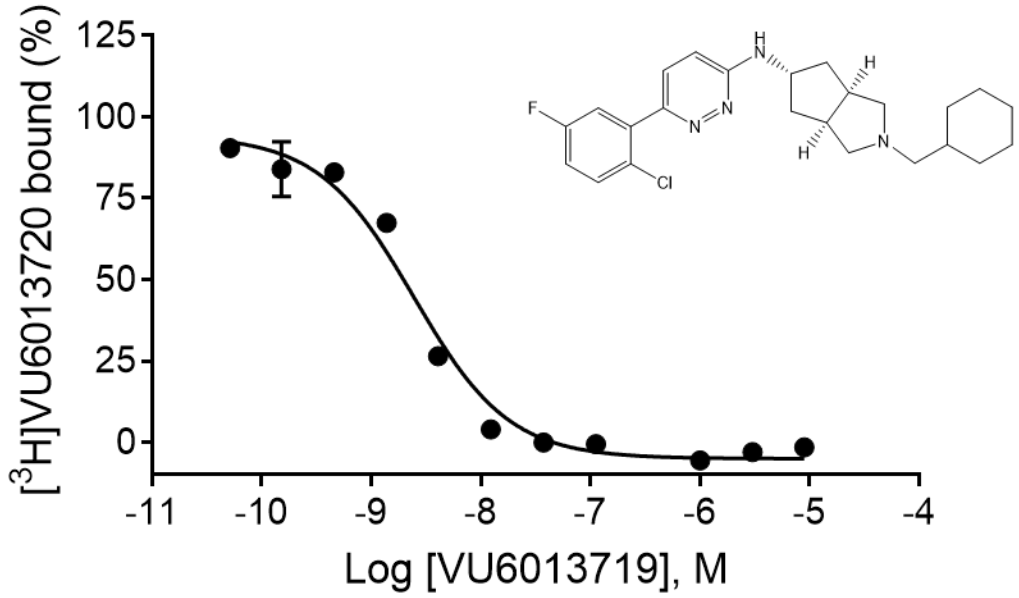

Supplemental Figure 1. VU6013719 fully competes for binding of [^{3}H]VU6013720. Increasing concentrations of VU6013719 were added with [^{3}H]VU6013720 to rat M_4-expressing cells. Data are the Mean ± SD from a representative assay of three independent experiments performed in triplicate.

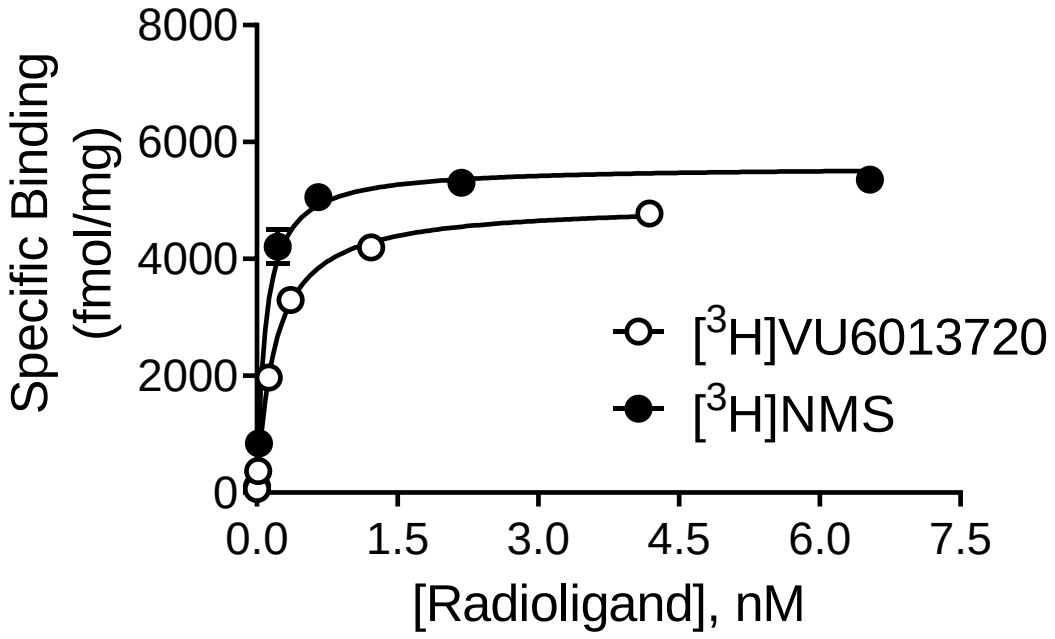

Supplemental Figure 2. [^{3}H]VU6013720 and [^{3}H]NMS label a similar number of sites in M_4-expressing cells. Increasing concentrations of [^{3}H]VU6013720 (white) or [^{3}H]NMS (black) were added to membranes from rat M_4 cells and specific binding was assessed. B_{max} values were 4500 ± 700 with [^{3}H]NMS and 4100 ± 500 fmol/mg with [^{3}H]VU6013720, and pK_d values were 10 ± 0.1 with [^{3}H]NMS and 9.6 ± 0.3 with [^{3}H]VU6013720, respectively. Data represent Mean ± SD performed three times in triplicate; data shown are representative of a single experiment.

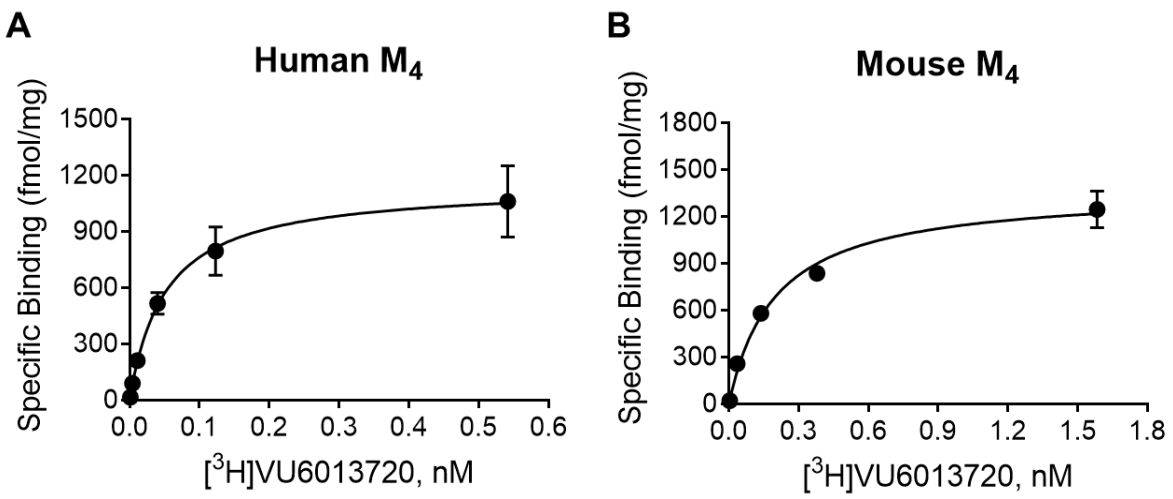

Supplemental Figure 3. [^{3}H]VU6013720 specifically binds to the human and mouse M_4 receptors. Specific binding of [^{3}H]VU6013720 to human (A) and mouse (B) M_4 receptors was evaluated using saturation binding assays, as described in Methods and Figure 3. [^{3}H]VU6013720 binds to human and mouse M_4 receptors with high affinity and in a saturable manner (refer to Table 2 for affinities). Data are the Mean ± SD from four experiments performed in quadruplicate (human) and 1 assay (mouse) performed in triplicate. Atropine was used as the nonspecific binding control.

Supplemental Methods

Synthesis of VU6013719.

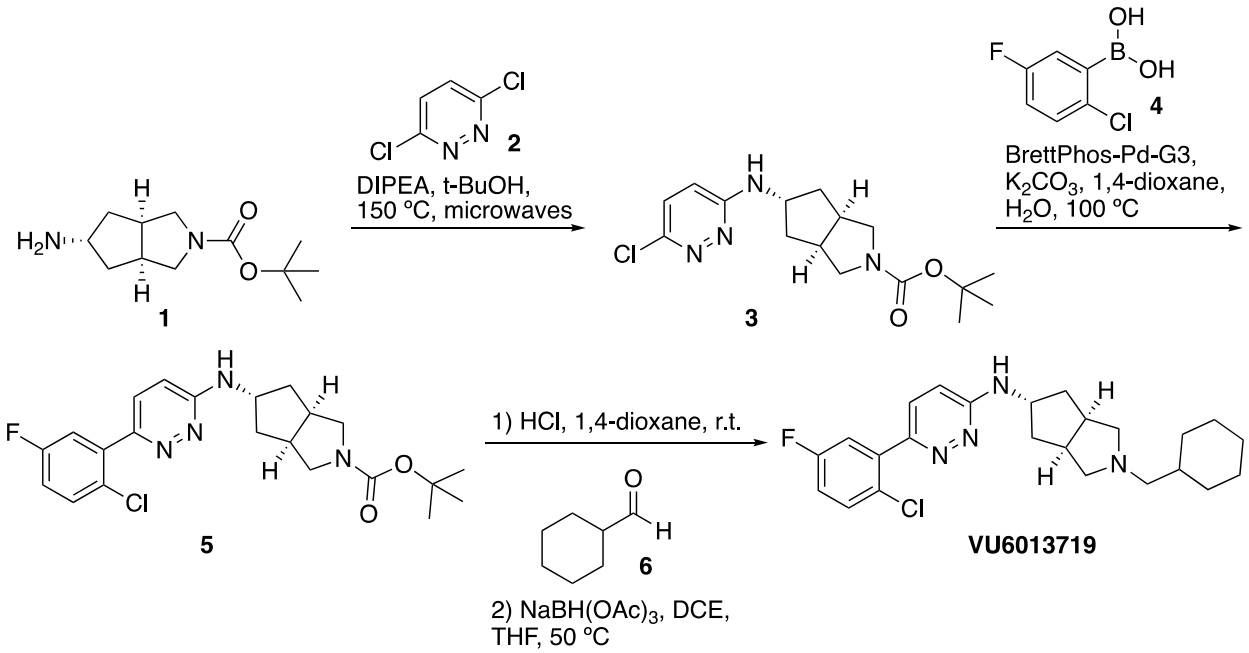

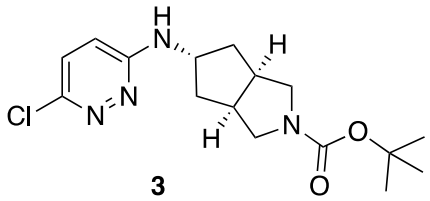

3

tert-butyl (3a*R*,5*s*,6a*S*)-5-((6-chloropyridazin-3-yl)amino)hexahydrocyclopenta[c]pyrrole-2(1*H*)-carboxylate (**3**) was prepared in a similar manner as Intermediate 3 from (Moehle, Bender et al. 2021). *tert*-butyl (3a*R*,5*s*,6a*S*)-5-aminohexahydrocyclopenta[*c*]pyrrole-2(1*H*)-carboxylate (**1**, 5.0 g, 22.1 mmol, 1 eq) and 3,6-dichloropyridazine (**2**, 9.87 g, 66.3 mmol, 3 eq) were combined in *tert*-butanol (40 mL) and DIPEA (11.5 mL, 66.3 mmol, 3 eq) was added. The resulting solution was heated to 150 °C under microwave irradiation for 2 h, after which time the reaction mixture was concentrated under reduced pressure, and crude residue was purified by normal phase

column chromatography on silica gel (3-100% EtOAc in hexanes) to give the title compound as a tan solid (4.82 g, 64%). ^{1}H-NMR (400 MHz, MeOD) δ 7.27 (d, *J* = 9.4 Hz, 1H), 6.87 (d, *J* = 9.4 Hz, 1H), 4.41 (p, *J* = 6.3 Hz, 1H), 3.55 (dd, *J* = 11.1, 8.0 Hz, 2H), 3.19 (dd, *J* = 11.4, 3.8 Hz, 2H), 2.90 – 2.80 (m, 2H), 1.90 – 1.92 (m, 2H), 1.89 – 1.81 (m, 2H), 1.46 (s, 9H). ^{13}C-NMR (101 MHz, MeOD) δ 159.3, 156.3, 146.8, 130.3, 120.5, 80.8, 53.7, 53.2 (signal broadening is observed), 42.3 (signal broadening is observed), 39.5, 28.8; ES-MS $[M+H\text{-}t\text{-}butyl]^{+}$ = 283.2.

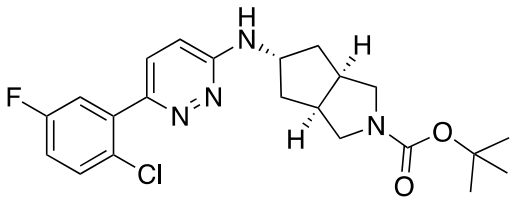

5

tert-butyl (3a*R*,5*s*,6a*S*)-5-((6-(2-chloro-5-fluorophenyl)pyridazin-3-yl)amino)hexahydrocyclopenta[c]pyrrole-2(1*H*)-carboxylate (5). *tert*-butyl (3a*R*,5*s*,6a*S*)-5-((6-chloropyridazin-3-yl)amino)hexahydrocyclopenta[c]pyrrole-2(1*H*)-carboxylate (**3**, 102 mg, 0.3 mmol, 1.0 eq), 2-chloro-5-fluorophenylboronic acid (**4**, 68.0 mg, 0.39 mmol, 1.3 eq), potassium carbonate (126 mg, 0.9 mmol, 3.0 eq) and BrettPhos-Pd-G3 (27.2 mg, 0.03 mmol, 0.1 eq) were combined in a flask, and 1,4-dioxane (2.4 mL) and water (0.6 mL) were added. The resulting mixture was evacuated and purged with nitrogen (3x). The resulting mixture was stirred under an inert atmosphere at 100 °C. After 2 h, the reaction mixture was diluted with EtOAc, filtered through a pad of Celite which was rinsed thoroughly with EtOAc, and the filtrate was concentrated under reduced pressure. The crude residue was purified using normal phase column chromatography on silica gel (0-100% EtOAc in hexanes) to provide the title compound as a pale-yellow powder (84 mg, 64%). ^{1}H NMR (400 MHz, DMSO) δ 7.61 (dd, *J* = 8.9, 5.2 Hz, 1H), 7.54 (d, *J* = 9.3 Hz, 1H), 7.44 (dd, *J* = 9.3, 3.1 Hz, 1H), 7.33 (ddd, *J* = 8.8, 8.1, 3.2 Hz, 1H), 7.17 (d, *J* = 6.7 Hz, 1H), 6.86 (d, *J* = 9.3 Hz, 1H), 4.45 (h, *J* = 6.6 Hz, 1H), 3.49 (dd, *J* = 11.1, 8.2 Hz, 2H), 3.30 (s, 2H),

3.09 (dd, *J* = 11.5, 3.7 Hz, 2H), 1.90 (ddd, *J* = 12.7, 6.3, 3.3 Hz, 2H), 1.83 – 1.72 (m, 2H), 1.40 (s, 9H); ^{13}C NMR (101 MHz, DMSO) δ 160.8 (d, *J* = 246.4 Hz), 157.7, 153.5, 149.0 (d, *J* = 2.0 Hz), 138.9 (d, *J* = 8.1 Hz), 131.7 (d, *J* = 9.1 Hz), 128.3, 126.7 (d, *J* = 2.0 Hz), 117.8 (d, *J* = 24.2 Hz), 116.9 (d, *J* = 22.2 Hz), 113.5, 78.3, 52.0 (signal broadening is observed), 51.7, 38.3, 28.2; ES-MS $[M+H]^+$ = 433.0.

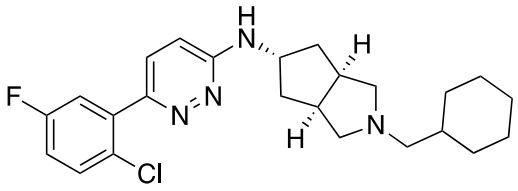

VU6013719

(3a*R*,5*s*,6a*S*)-*N*-(6-(2-chloro-5-fluorophenyl)pyridazin-3-yl)-2-(cyclohexylmethyl)octahydrocyclopenta[*c*]pyrrol-5-amine (VU6013719). tert-butyl (3a*R*,5*s*,6a*S*)-5-((6-(2-chloro-5-fluorophenyl)pyridazin-3-yl)amino)hexahydrocyclopenta[*c*]pyrrole-2(1*H*)-carboxylate (**5**, 83.6 mg, 0.19 mmol, 1.0 eq) was dissolved in 1,4-dioxane (1.9 mL). A solution of HCl in 1,4-dioxane (4M, 0.72 mL, 2.96 mmol, 15 eq) was added dropwise. After 2 h at r.t., the reaction mixture was concentrated under reduced pressure to give the HCl salt, which was dried under vacuum and carried forward without additional purification (71 mg). The HCl salt was suspended in DCE (2.0 mL) and THF (0.5 mL) and cyclohexanecarbaldehyde (64.7 mg, 0.58 mmol, 3.0 eq) was added. The resulting mixture was stirred at r.t. for 15 min and sodium triacetoxyborohydride (122 mg, 0.58 mmol, 3.0 eq.) was added. After 1 h at 50 °C, sat. $NaHCO_3$ solution was added to the reaction mixture, and the aqueous layer was extracted with DCM (3x). The combined organic extracts were washed with brine, dried over Na_2SO_4, filtered and concentrated. Purification using normal phase chromatography on silica gel (0-10% MeOH in DCM) provided the title compound (56 mg, 68% over 2 steps); ^{1}H NMR (400 MHz, DMSO) δ 7.61 (dd, *J* = 8.9, 5.2 Hz, 1H), 7.53 (d, *J* = 9.3 Hz,

1H), 7.44 (dd, *J* = 9.3, 3.1 Hz, 1H), 7.32 (ddd, *J* = 8.8, 8.1, 3.2 Hz, 1H), 7.04 (d, *J* = 6.9 Hz, 1H), 6.83 (d, *J* = 9.3 Hz, 1H), 4.49 – 4.41 (m, 1H), 2.67 – 2.61 (m, 1H), 2.50 – 2.46 (m, 2H), 2.31 – 2.23 (m, 2H), 2.15 (d, *J* = 7.2 Hz, 2H), 1.86 – 1.75 (m, 4H), 1.70 – 1.57 (m, 5H), 1.46 – 1.35 (m, 1H), 1.28 – 1.08 (m, 3H), 0.89 – 0.79 (m, 2H); ^{13}C NMR (101 MHz, DMSO) δ 160.8 (d, *J* = 246.4 Hz), 157.9, 148.9 (d, *J* = 2.0 Hz), 138.9 (d, *J* = 8.1 Hz), 131.6 (d, *J* = 9.1 Hz), 128.3, 126.6 (d, *J* = 2.0 Hz), 117.8 (d, *J* = 24.2 Hz), 116.8 (d, *J* = 22.2 Hz), 113.4, 62.4, 61.9, 52.0, 36.4, 31.4, 26.4, 25.6; ES-MS $[M+H]^+$ = 429.1.